

Model predictive control with fractional-order delay compensation for fast sampling systems

Ze ZHOU¹, Zhitao LIU^{1*}, Hongye SU¹ & Liyan ZHANG²¹State Key Laboratory of Industrial Control Technology, Institute of Cyber-Systems and Control, Zhejiang University, Hangzhou 310027, China;²School of Automation, Wuhan University of Technology, Wuhan 430070, China

Received 18 June 2020/Revised 15 August 2020/Accepted 1 October 2020/Published online 20 May 2021

Abstract Model predictive control (MPC) is widely used in fast sampling systems owing to its fast regulating ability. However, the sampling delay is a key issue and tends to be a fractional multiple of the sampling period. If the fractional-order delay is not accurately offset, the controller output will exhibit errors, thus resulting in oscillations in controlled system. Moreover, the MPC delay compensation algorithm is limited to the computation time. To address the problems of fractional delay and computational burden in fast sampling systems, we propose a new method to compensate for the fractional-order sampling delay. First, we use a finite-impulse-response fractional delay filter based on a Lagrange interpolation polynomial to approximate the fractional portion. Moreover, we prove that high accuracy and simplicity can be ensured when the polynomial order is one. Then, we estimate the current state variable using the delayed sampling signal and control signals of past moments. Further, we obtain the current control signal according to the estimated state variable. By considering the simultaneous existence of computational and sampling delays, a full compensation strategy is proposed. Computational simulation results validate the proposed MPC algorithm with fractional-order delay compensation and demonstrate its advantages.

Keywords model predictive control, fast sampling systems, sampling delay, fractional-order, Lagrange interpolation polynomial

Citation Zhou Z, Liu Z T, Su H Y, et al. Model predictive control with fractional-order delay compensation for fast sampling systems. *Sci China Inf Sci*, 2021, 64(7): 172211, <https://doi.org/10.1007/s11432-020-3096-0>

1 Introduction

In each sampling period, model predictive control (MPC) constructs and solves the optimization problem, thus forming an optimal control method [1]. Indeed, MPC considers both control and optimization and has been successfully used in the process industries [2]. In controlled systems, the time delay is a significant factor that cannot be overlooked [3, 4]. To solve the delay problem in slow sampling systems, numerous effective MPC compensation methods have been successfully used [5, 6]. For uncertain time-varying systems with state delay, Jeong et al. [7] proposed an improved MPC algorithm to stabilize the closed-loop system and verified the effectiveness of the proposed method using a numerical example of a computer-simulated truck trailer with a sampling time of 0.1 s. By considering asynchronous measurement and delay, the distributed MPC was verified using a chemical process example with a sampling time of 0.035 h [8]. Considering a time-delay continuous-stirred tank reactor system as an example, the effectiveness of the iteratively distributed MPC [9] and fuzzy MPC [10] was verified. Most researchers have focused on traditional process control fields, including refining, petrochemical, and chemical industries. The sampling cycles of these systems are long, and the requirements of the MPC algorithm are not arduous. However, in fast sampling systems, such as power electronics, the sampling period is short and there is a high requirement for MPC control accuracy and rapid real-time calculation.

Currently, MPC has also been gradually adopted in fast sampling systems [11–13]. Considering the delay caused by the calculation time in MPC, Cortes et al. [14] presented a simple and effective compensation method, which shifts one step forward and outputs the optimal control signal at the next moment.

* Corresponding author (email: ztliu@zju.edu.cn)

Moreover, a networked fuzzy MPC with a small computational cost was developed to ensure the robustness of the system with delay [15]. To address the problems of sampling delay, Zhang et al. [16] proposed a multistep integer compensation MPC algorithm that could effectively improve the system performance.

The time delay can be classified into computation delay and sampling delay. First, we discuss the computational delay. The control signal calculation must be completed within one cycle, so the computational delay will not exceed one cycle. Whether the computation delay is an integer or a fraction, it can be treated as an integer delay. At the current moment, the optimal control signal at the next moment is calculated in advance and then outputted at the next sampling moment [14]. Therefore, the computational delay compensation is simple and has little impact on the algorithm complexity. However, the sampling delay must distinguish between integers and fractions. Generally, the processing method of the sampling delay is to adopt multiple periods of integer compensation. Either one-step or multistep compensation is directly considered. However, integer compensation is challenging with the fractional-order delay, causing oscillations in controlled systems. On the one hand, in fast sampling systems, the control signal must complete the calculation within one sampling period. On the other hand, the MPC algorithm, which is improved to compensate for the impact of the sampling delay, will increase the computational burden, particularly the sampling delay of a fractional multiple of the sampling period. Therefore, an effective low-computation compensation algorithm is particularly significant.

Several researchers have examined the fractional delay in digital filters [17–19]. Based on the concept of a finite-impulse-response (FIR) filter using a Lagrange interpolation polynomial, Zou et al. [20] proposed a real-time frequency adaptive control method to eliminate harmonic distortions with changing grid frequency. For the fractional-order sampling delay problem, Bagheri et al. [21] designed a tuning method for MPC of the first-order plus a fractional dead time model. However, the model was limited to a first-order system. In fast sampling systems, such as power electronic systems, the model order is often greater than one, presenting a high-order form. Compared with [21], the model proposed in this paper has more general applicability.

For fast sampling systems, the existing literature mainly focuses on the integer-order multiple sampling delays with little attention to the fractional-order sampling delay compensation of MPC. The main contributions of this paper relative to the existing studies are as follows. We propose an MPC algorithm with fractional-order sampling delay compensation to improve the performance of MPC in fast sampling systems and utilize the FIR fractional delay filter based on Lagrange interpolation to approximate the fractional sampling delay. Moreover, we prove that when the polynomial order n is one, the complexity is the lowest and the approximation accuracy is sufficiently high at low frequencies. The low computational complexity can ensure that the calculation is completed in a limited time, and high accuracy can ensure good approximation of the fractional sampling delay. Therefore, the low-complexity and high-accuracy MPC algorithm proposed in this paper can be well applied to fast sampling systems. Moreover, by considering the computation delay, we propose a full compensation strategy for the coexistence of computational and sampling delays. Further, the closed-loop stability of the system is discussed. Finally, the simulation results verify the efficiency of the proposed fractional-order compensation algorithm.

The remainder of this paper is structured as follows. Section 2 presents the problem description. Section 3 describes the controller design for fractional-order delay systems. Section 4 reviews the stability analysis. Section 5 presents the simulation results, demonstrating the efficiency of MPC with fractional-order delay compensation in fast sampling systems. Finally, conclusions are presented in Section 6.

Notation. For a matrix M , $[M]^i$ denotes the i th row. For a vector a , $[a]_i$ denotes the i th component. $A \succ 0$ ($A \prec 0$) means that matrix A is positive (negative) definite.

2 Problem description

Consider the system

$$\begin{cases} x(k+1) = Ax(k) + Bu(k) + F, \\ y(k) = Cx(k), \end{cases} \quad (1)$$

where $x \in \mathbb{R}^{N_n}$, $u \in \mathbb{R}^{N_u}$, and $y \in \mathbb{R}^{N_y}$ are state variable, control signal, and output variable, respectively; $A \in \mathbb{R}^{N_n \times N_n}$, $B \in \mathbb{R}^{N_n \times N_u}$, and $C \in \mathbb{R}^{N_y \times N_n}$ denote coefficient matrices, respectively; $F \in \mathbb{R}^{N_n}$ is a parameter matrix.

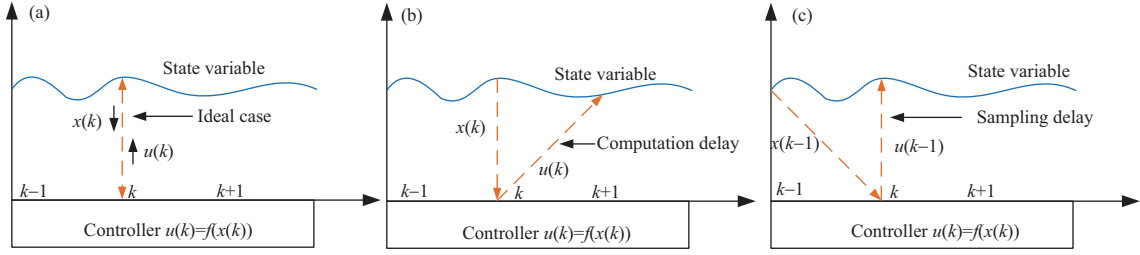


Figure 1 (Color online) (a) Ideal case without delay; (b) computation delay; (c) sampling delay.

For the system (1), we assume that the functional relationship between the optimal control signal and the state variable is $u(k) = f(x(k))$ where $u(k)$ and $x(k)$ are the control signal and state variable, respectively. Moreover, we take the one-cycle computation delay and one-cycle sampling delay as examples to illustrate the impact of the two on the system. In the ideal no-delay state presented in Figure 1(a), at the current moment k , the sampled state variable is $x(k)$ and the control signal $u(k)$ acts on the system. In this case, the controlled system can operate stably. Figure 1(b) shows the case with only the computation delay. Due to the delay, $u(k)$ calculated at the current moment k acts on the system at moment $k + 1$, which causes the control law to form one cycle lag. In addition, Figure 1(c) presents the situation where only the sampling delay exists. What is sampled at the current moment k is the state variable $x(k - 1)$, so the control law $u(k - 1)$ is corresponding to the previous moment, which is also equivalent to the control law forming one cycle lag. Whether it is the existence of calculation delay or sampling delay, it will cause the control law to lag, which has a bad influence on the controlled system. Therefore, it is necessary to compensate for the system delay. Indeed, the delay is generally not an integer sampling period, so we must consider the compensation algorithm of the fractional-order delay.

3 Controller design for the fractional-order delay system

We first consider the solution of the system (1). Indeed, the prediction equation is given by

$$Y(k) = S_x x(k) + S_u U(k) + D_F, \quad (2)$$

where $Y(k)$, $U(k)$, S_x , S_u , and D_F are

$$Y(k) = \begin{bmatrix} y(k+1|k) \\ y(k+2|k) \\ \vdots \\ y(k+N_p|k) \end{bmatrix}_{N_p \times 1}, \quad U(k) = \begin{bmatrix} u(k|k) \\ u(k+1|k) \\ \vdots \\ u(k+N_m-1|k) \end{bmatrix}_{N_m \times 1},$$

$$S_x = \begin{bmatrix} CA \\ CA^2 \\ CA^3 \\ \vdots \\ CA^{N_p} \end{bmatrix}_{N_p \times 1}, \quad D_F = \begin{bmatrix} CF \\ CAF + CF \\ \vdots \\ \sum_{i=0}^{N_p-1} CA^{N_p-i-1}F \end{bmatrix}_{N_p \times 1},$$

$$S_u = \begin{bmatrix} CB & 0 & 0 & \cdots & 0 & 0 \\ CAB & CB & 0 & \cdots & 0 & 0 \\ \vdots & \vdots & \vdots & \vdots & \vdots & \vdots \\ CA^{N_m-1}B & CA^{N_m-2}B & \cdots & \cdots & CAB & CB \\ \vdots & \vdots & \vdots & \vdots & \vdots & \vdots \\ CA^{N_p-1}B & CA^{N_p-2}B & \cdots & \cdots & CA^{N_p-N_m+1}B & \sum_{i=0}^{N_p-N_m} CA^{N_p-N_m-i}B \end{bmatrix}_{N_p \times N_m},$$

where N_p and N_m are predictive horizon and control horizon, respectively; moreover, $N_p \geq N_m$. Define the objective function

$$\begin{aligned} J(U(k)) &= (Y(k) - R_y)^T W_y (Y(k) - R_y) + (U(k) - R_u)^T W_u (U(k) - R_u) \\ &= \frac{1}{2} U(k)^T \Psi U(k) + g^T U(k) + \varphi_{\text{con}}, \end{aligned} \tag{3}$$

where $R_y, R_u \in \mathbb{R}$ represent reference values of the controlled variable and control signal, respectively; W_y and W_u are diagonal weight matrices. Let

$$\begin{aligned} \psi_J &= S_x x(k) + D_F, \\ \Psi &= 2(S_u^T W_y S_u + W_u), \\ g^T &= 2((\psi_J - R_y)^T W_y S_u - R_u^T W_u), \\ \varphi_{\text{con}} &= (\psi_J - R_y)^T W_y (\psi_J - R_y) + R_u^T W_u R_u. \end{aligned} \tag{4}$$

Since φ_{con} is a constant independent of $U(k)$, we are able to obtain a new objective function given by

$$\min_{U(k)} J_n(U(k)) = \frac{1}{2} U(k)^T \Psi U(k) + g^T U(k). \tag{5}$$

Supposing $\Psi > 0$, the solution can be expressed as

$$U(k) = -\Psi^{-1} g. \tag{6}$$

We substitute (4) into (6) to get

$$U(k) = -\Psi^{-1} S_u^T W_y S_x x(k) - 2\Psi^{-1} (S_u^T W_y (D_F - R_y) - W_u R_u). \tag{7}$$

Defining $u(k) = [U(k)]_1$, $M = [-\Psi^{-1} S_u^T W_y S_x]_1$, and $b = [-2\Psi^{-1} (S_u^T W_y (D_F - R_y) - W_u R_u)]_1$, we are able to derive the optimal control signal as follows:

$$u(k) = Mx(k) + b, \tag{8}$$

where M is a vector and b is a scalar.

3.1 Fractional-order compensation of computation delay

The state-space model with the computation delay is

$$\begin{cases} x(k+1) = Ax(k) + Bu(k - d_c) + F, \\ y(k) = Cx(k), \end{cases} \tag{9}$$

where d_c is the delay term. Since the computation delay does not exceed one cycle, d_c belongs to $[0,1]$. Considering only the computation delay, we propose the Algorithm 1 and express the future trajectory $y(k+1+N_p|k)$ as follows:

$$y(k+1+N_p|k) = CA^{N_p+1}x(k) + \sum_{i=-1}^{N_p-1} CA^{N_p-i-1}Bu(k+1+i|k) + \sum_{i=-1}^{N_p-1} CA^{N_p-i-1}F. \tag{10}$$

Algorithm 1 Fractional-order compensation of the computation delay

- 1: Obtain the state variables of the current moment;
 - 2: Apply the optimal control signal $u(k)$ calculated before one period to the current time;
 - 3: At the current time k , calculate the optimal control signal $u(k+1)$ and output it at time $k+1$.
-

Since $y(k+1)$ can be calculated from known $x(k)$ and $u(k)$, we start to predict from $k+2$ moment. Accordingly, the prediction equation can be described as

$$Y(k) = S_x x(k) + S_u U(k) + D_u u(k) + D_F, \tag{11}$$

where $Y(k)$, $U(k)$, S_x , D_u , and D_F are

$$Y(k) = \begin{bmatrix} y(k+2|k) \\ y(k+3|k) \\ \vdots \\ y(k+N_p+1|k) \end{bmatrix}_{N_p \times 1}, \quad U(k) = \begin{bmatrix} u(k+1|k) \\ u(k+2|k) \\ \vdots \\ u(k+N_m|k) \end{bmatrix}_{N_m \times 1},$$

$$S_x = \begin{bmatrix} CA^2 \\ CA^3 \\ \vdots \\ CA^{N_p+1} \end{bmatrix}_{N_p \times 1}, \quad D_u = \begin{bmatrix} CAB \\ CA^2B \\ \vdots \\ CA^{N_p}B \end{bmatrix}_{N_p \times 1}, \quad D_F = \begin{bmatrix} \sum_{i=-1}^0 CA^{-i}F \\ \sum_{i=-1}^1 CA^{1-i}F \\ \vdots \\ \sum_{i=-1}^{N_p-1} CA^{N_p-i-1}F \end{bmatrix}_{N_p \times 1}.$$

We redefine $\psi_J = S_x x(k) + D_u u(k) + D_F$ in (4) and substitute S_x , D_u , and D_F in (11) to (4). In the same derivation way as (8), we can get the optimal solution of the controller as follows:

$$u(k+1) = M_1 x(k) + b_1. \tag{12}$$

Here, $M_1 = [-\Psi^{-1} S_u^T W_y S_x]^1$, and $b_1 = [-2\Psi^{-1} (S_u^T W_y (D_F - R_y) - W_u R_u)]_1$.

3.2 Fractional-order compensation of sampling delay

MPC takes the state variable $x(k)$ sampled at the current moment k as the starting point of prediction. Correspondingly, the calculation of the control law $u(k)$ is related to $x(k)$. For fractional sampling delay $x(k - \tau)$, we need to estimate the current state variable $x(k)$ according to $x(k - \tau)$ where $\tau = N + d$, $N = \text{int}[\tau]$, and $d \in [0, 1)$. To achieve this goal, we first analyze the integer delay compensation. If the sampling signal is delayed by integer multiple periods, then the estimated value $x(k|k - N)$ can be deduced as

$$x(k|k - N) = A^N x(k - N) + \sum_{i=1}^N A^{i-1} B u(k - i) + \sum_{i=1}^N A^{i-1} F. \tag{13}$$

Eq. (13) gives us an inspiration that we can establish the relationship between fractional sampling delay $x(k - \tau)$ and integer sampling delay $x(k - N)$. Once we have constructed the relationship between $x(k - \tau)$ and $x(k - N)$, then we can get the estimated value $x(k|k - \tau)$ based on (13). The polynomial interpolation is a considerable approach that can be utilized to approximate the fractional-order delay z^{-d} . Compared to other interpolation methods, the Lagrange interpolation method has the following advantages: easy explicit formulas for the coefficients, great response at low frequency bands, and a smooth magnitude response [22]. Indeed, there are other polynomial interpolation methods for the fractional-order delay approximation, such as splines interpolation. However, these methods are not optimal from the frequency domain perspective [22]. According to [20], it is known that fractional-order delay z^{-d} can be approximated by a Lagrange-interpolation-based filter as follows:

$$z^{-d} \approx \sum_{j=0}^n \alpha_j z^{-j}, \tag{14}$$

$$\alpha_j = \prod_{\substack{i=0 \\ i \neq j}}^n \frac{d-i}{j-i}, \quad i, j = 0, 1, \dots, n \quad (n \geq 1), \tag{15}$$

where n is polynomial order. Ref. [20] indicates that the Lagrange-interpolation-based FIR fractional delay filter has high approximation accuracy within its bandwidth, i.e., the logarithmic magnitude of the filter frequency characteristic is close to 0 dB. In other words, the filter has high approximation

accuracy in the low-frequency range. Further, we use the following theorem to prove that $n = 1$ can ensure the lowest computational complexity of $x(k|k - \tau)$ and the fractional delay filter bandwidth is $[0, f_s/4]$, $\forall d \in [0, 1)$ where f_s denotes the sampling frequency. It is noted that the bandwidth of the low pass filter is $[0, f_c]$ where f_c is the cut-off frequency. We know that the cut-off frequency f_c refers to the point where the logarithmic magnitude of the frequency characteristic is -3 dB. Moreover, the logarithmic magnitude of -3 dB is equal to the absolute magnitude of $\frac{1}{\sqrt{2}}$.

Theorem 1. (1) $n = 1$ can ensure the lowest computational complexity of $x(k|k - \tau)$. (2) When $n = 1$, if $A_\beta(\omega) \geq \frac{1}{\sqrt{2}}$, $\forall d \in [0, 1)$, the frequency of the excitation signal satisfies

$$0 \leq f \leq \frac{f_s}{4}, \tag{16}$$

where $A_\beta(\omega)$ is the magnitude frequency characteristic function of the FIR filter; f denotes the excitation signal frequency.

Proof. (1) According to (14), we can transform $x(k - \tau)$ into

$$x(k - \tau) = z^{-\tau}x(k) = z^{-(N+d)}x(k) = z^{-N} \left(\sum_{j=0}^n \alpha_j z^{-j} \right) x(k) = \sum_{j=0}^n \alpha_j x(k - (N + j)). \tag{17}$$

According to (1), we know that the sum of the last two terms $\alpha_{n-1}x(k - (N + n - 1))$ and $\alpha_n x(k - (N + n))$ in $\sum_{j=0}^n \alpha_j x(k - (N + j))$ is

$$\begin{aligned} & \alpha_{n-1}x(k - (N + n - 1)) + \alpha_n x(k - (N + n)) \\ &= (\alpha_{n-1}I_m + \alpha_n A^{-1})x(k - (N + n - 1)) - \alpha_n A^{-1}(Bu(k - (N + n)) + F), \end{aligned} \tag{18}$$

where I_m is the identity matrix of the same order as A . Rearranging (17), we are able to derive

$$\begin{aligned} & x(k - \tau) + \alpha_n A^{-1}(Bu(k - (N + n)) + F) \\ &= \sum_{j=0}^{n-2} \alpha_j x(k - (N + j)) + (\alpha_{n-1}I_m + \alpha_n A^{-1})x(k - (N + n - 1)). \end{aligned} \tag{19}$$

Indeed, we eliminate $x(k - (N + n))$. Similarly, we can replace $x(k - (N + n - 1))$ with $x(k - (N + n - 2))$. After many iterations, we finally obtain the relationship between $x(k - \tau)$ and $x(k - N)$ as follows:

$$x(k - \tau) + \sum_{i=1}^n \left(\sum_{j=i}^n \alpha_j A^{i-j-1} \right) (Bu(k - (N + i)) + F) = \sum_{j=0}^n \alpha_j A^{-j} x(k - N). \tag{20}$$

Then, we are able to get $x(k - N)$ described as

$$x(k - N) = \left(\sum_{j=0}^n \alpha_j A^{-j} \right)^{-1} \left(x(k - \tau) + \sum_{i=1}^n \left(\sum_{j=i}^n \alpha_j A^{i-j-1} \right) (Bu(k - (N + i)) + F) \right). \tag{21}$$

Based on (13) as well as (21), we can derive

$$\begin{aligned} x(k|k - \tau) &= A^N \left(\left(\sum_{j=0}^n \alpha_j A^{-j} \right)^{-1} \left(x(k - \tau) + \sum_{i=1}^n \left(\sum_{j=i}^n \alpha_j A^{i-j-1} \right) (Bu(k - (N + i)) + F) \right) \right) \\ &+ \sum_{i=1}^N A^{i-1} Bu(k - i) + \sum_{i=1}^N A^{i-1} F. \end{aligned} \tag{22}$$

$x(k|k - \tau)$ needs to be updated in real-time during each sampling period and, thus, $n = 1$ can guarantee the low complexity of $x(k|k - \tau)$ due to $n \geq 1$.

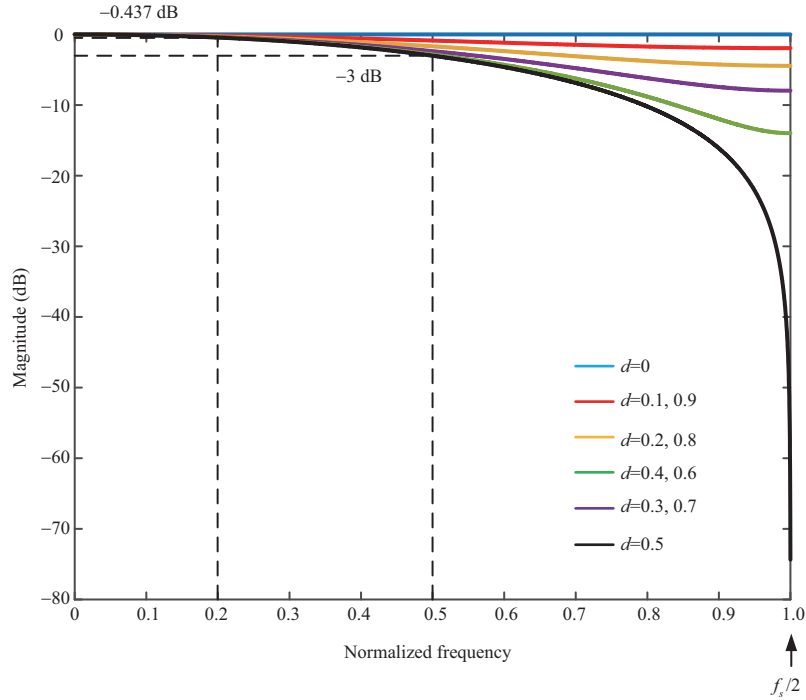


Figure 2 (Color online) Magnitude frequency characteristics of Lagrange-interpolation-based fractional delay filters with order $n = 1$.

(2) The expression of the Lagrange interpolation FIR fractional delay filter is $G(z) = 1 - d + dz^{-1}$ if $n = 1$. Indeed, the mapping is $z = e^{sT_s}$ between z and s . By substituting $z = e^{sT_s}$ into $G(z)$, we can deduce $G_c(s) = 1 - d + de^{-sT_s}$. Assuming $s = j\omega$, we have

$$G_c(j\omega) = 1 - d + de^{-j\omega T_s}.$$

Define the magnitude of $G_c(j\omega)$ as

$$A_\beta(\omega) = \sqrt{(1 - d + d \cos(\omega T_s))^2 + (d \sin(\omega T_s))^2} = \sqrt{(1 - d)^2 + d^2 + 2(1 - d)d \cos(\omega T_s)}.$$

Moreover, define $H_\beta(d) = (1 - d)^2 + d^2 + 2(1 - d)d \cos(\omega T_s)$ and the derivative of $H_\beta(d)$ is

$$\dot{H}_\beta(d) = (4 - 4 \cos(\omega T_s))d + 2 \cos(\omega T_s) - 2.$$

We consider only positive frequency and combine the Shannon sampling theorem to obtain $0 \leq \omega \leq \frac{\omega_s}{2} = \frac{\pi}{T_s}$. Therefore, $A_\beta(\omega)$ is a monotonically decreasing function if $d \in (0, 1)$. First, $\omega = 0$ can deduce $A_\beta(\omega) = 1$. Then, if $d = 0$, $A_\beta(\omega)$ is also equal to one. Finally, for any $d \in [0, 1)$, $A_\beta(\omega) = 1 \geq \frac{1}{\sqrt{2}}$ if $\omega = 0$. Now we will analyze $0 < \omega \leq \frac{\omega_s}{2}$, and we have $\cos(\omega T_s) \in [-1, 1)$. The coefficient $4 - 4 \cos(\omega T_s)$ of d is always greater than 0 with $\cos(\omega T_s) \in [-1, 1)$. $H_\beta(d)$ will get the minimum value at $d = 0.5$. Let $d := 1 - d$, and we can know $H_\beta(d) = H_\beta(1 - d)$. It shows that $H_\beta(d)$ is symmetrical at $d = 0.5$. $A_\beta(\omega) \geq \frac{1}{\sqrt{2}}$ for any $d \in [0, 1)$ can infer

$$\min_d H_\beta(d) \geq \frac{1}{2}.$$

Because of $\min_d H_\beta(d) = H_\beta(0.5) = \frac{1}{2} + \frac{1}{2} \cos(\omega T_s) \geq \frac{1}{2}$, we have $\cos(\omega T_s) \geq 0$ and derive $0 < \omega T_s \leq \frac{\pi}{2}$. Further, $0 < \omega T_s \leq \frac{\pi}{2}$ can deduce $0 < \omega \leq \frac{\omega_s}{4}$. To sum up, the range of ω satisfying good approximation accuracy is $[0, \frac{\omega_s}{4}]$. Due to $\omega = 2\pi f$, $0 \leq f \leq \frac{f_s}{4}$ is proved.

We get the logarithmic magnitude frequency characteristic curves of (14) as shown in Figure 2. The Nyquist frequency is half of the sampling frequency f_s . Figure 2 presents that the filter has high accuracy in the bandwidth frequency range. Further, if the signal frequency is in $[0, f_s/10]$, the logarithmic magnitude of frequency characteristic is in $[-0.437, 0]$ dB and its maximum drop is 0.437 dB. This

indicates that the lower frequency has higher accuracy. Taking fast sampling systems such as power electronics as an example, the sampling frequency is generally set to 20 kHz. Then, if the signal frequency is in [0, 5] kHz, it is considered to have high approximation accuracy. If the signal frequency range is smaller, for example in [0, 2] kHz, the approximation accuracy is higher.

According to Theorem 1, we substitute $n = 1$ into (22) to derive

$$x(k|k - \tau) = A^N((\alpha_0 I_m + \alpha_1 A^{-1})^{-1}(x(k - \tau) + \alpha_1 A^{-1}(Bu(k - (N + 1)) + F))) + \sum_{i=1}^N A^{i-1}Bu(k - i) + \sum_{i=1}^N A^{i-1}F. \tag{23}$$

If τ is an integer, (23) and (13) are equivalent. If τ is a fraction, we can substitute $x(k|k - \tau)$ in (23) for $x(k)$ in (8), and obtain the optimal control signal

$$u(k) = Mx(k|k - \tau) + b. \tag{24}$$

Accordingly, the fractional-order compensation of sampling signal delay is listed in Algorithm 2. Then, we synthesize the computation delay and sampling delay. Similarly, we substitute $x(k|k - \tau)$ in (23) for $x(k)$ in (12) and derive

$$u(k + 1) = M_1x(k|k - \tau) + b_1. \tag{25}$$

Algorithm 2 Fractional-order compensation of sampling signal delay

- 1: Calculate M and b in (8);
 - 2: Estimate the current state variable $x(k|k - \tau)$ by (23);
 - 3: Obtain the optimal control law by (24).
-

In summary, the compensation algorithm of the hybrid delay (coexistence of computational and sampling delays) proposed in this paper is presented in Algorithm 3.

Algorithm 3 Fractional-order compensation of hybrid delay

- 1: Calculate M_1 and b_1 in (12);
 - 2: Estimate the current state variable $x(k|k - \tau)$ by (23);
 - 3: Obtain the optimal control law by (25).
-

4 Stability analysis

For (25), we assume $k := k - 1$ and have

$$u(k) = M_1x(k - 1|k - \tau - 1) + b_1. \tag{26}$$

To simplify the notation, we replace $x(k - 1|k - \tau - 1)$ with $x(k - \tau_p)$ where $\tau_p = \tau + 1$. Substituting (26) into (1), we have

$$x(k + 1) = Ax(k) + B_Mx(k - \tau_p) + B_F, \tag{27}$$

where $B_M = BM_1$ and $B_F = Bb_1 + F$.

Theorem 2. The system (27) is asymptotically stable if there are symmetric positive definite matrices Q_1, Q_2 , and nonsingular matrix $\int_0^{T_s} e^{A_s\gamma}d\gamma$, which satisfies

$$\Phi = \begin{bmatrix} A_s^T Q_1 + Q_1 A_s + Q_2 & Q_1 A_s (A - I)^{-1} B_M \\ [A_s (A - I)^{-1} B_M]^T Q_1 & -Q_2 \end{bmatrix} \prec 0, \tag{28}$$

where A_s is the coefficient matrix of the continuous-time state vector. I is the unit matrix with the same dimension as A_s .

Proof. We convert (27) into a continuous form as follows:

$$\dot{x}(t) = A_s x(t) + B_{Ms} x(t - T_s \tau_p) + B_{Fs}, \tag{29}$$

where T_s is the sampling time of the discrete model. The coefficients of the continuous model and discrete model are transformed as follows:

$$\begin{cases} A = e^{A_s T_s}, \\ B_M = \int_0^{T_s} e^{A_s \gamma} d\gamma \cdot B_{Ms}, \\ B_F = \int_0^{T_s} e^{A_s \gamma} d\gamma \cdot B_{Fs}. \end{cases} \tag{30}$$

Assume that the equilibrium state of the system is x_e , and x_e satisfies the following expression:

$$(A_s + B_{Ms})x_e = -B_{Fs}. \tag{31}$$

We define a new state variable $q(t) = x(t) - x_e$, and the equilibrium state q_e of $q(t)$ is zero. Substitute $q(t)$ into (31) and we obtain

$$\dot{q}(t) = A_s q(t) + B_{Ms} q(t - T_s \tau_p). \tag{32}$$

Next, we construct a Lyapunov function

$$V(q(t)) = q^T(t) Q_1 q(t) + \int_{t-T_s \tau_p}^t q^T(\gamma) Q_2 q(\gamma) d\gamma, \tag{33}$$

where Q_1 and Q_2 are symmetric positive definite matrices. The derivative of $V(q(t))$ with respect to time t is

$$\dot{V}(q(t)) = 2q^T(t) Q_1 (A_s q(t) + B_{Ms} q(t - T_s \tau_p)) + q^T(t) Q_2 q(t) + q^T(t - T_s \tau_p) Q_2 q(t - T_s \tau_p). \tag{34}$$

We rewrite (34) and obtain

$$\dot{V}(q(t)) = \xi^T \Phi \xi, \tag{35}$$

where ξ and Φ are

$$\xi = \begin{bmatrix} q(t) \\ q(t - T_s \tau_p) \end{bmatrix}, \tag{36}$$

$$\Phi = \begin{bmatrix} A_s^T Q_1 + Q_1 A_s + Q_2 & Q_1 B_{Ms} \\ B_{Ms}^T Q_1 & -Q_2 \end{bmatrix}. \tag{37}$$

According to (30), we have

$$B_{Ms} = \left[\int_0^{T_s} e^{A_s \gamma} d\gamma \right]^{-1} B_M. \tag{38}$$

In addition, due to

$$\frac{d(e^{A_s t})}{dt} = A_s e^{A_s t} = e^{A_s t} A_s, \tag{39}$$

then the following formula is given by

$$\int_0^{T_s} e^{A_s \gamma} d\gamma = e^{A_s t} A_s^{-1} \Big|_0^{T_s} = (e^{A_s T_s} - I) A_s^{-1}. \tag{40}$$

Substituting (30) and (40) into (38), we can deduce

$$B_{Ms} = A_s (A - I)^{-1} B_M. \tag{41}$$

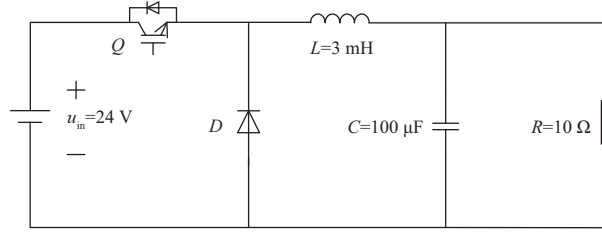


Figure 3 Topology and parameters of the BUCK converter.

We substitute (41) into (37) to derive

$$\Phi = \begin{bmatrix} A_s^T Q_1 + Q_1 A_s + Q_2 & Q_1 A_s (A - I)^{-1} B_M \\ [A_s (A - I)^{-1} B_M]^T Q_1 & -Q_2 \end{bmatrix}.$$

Therefore, the system (27) is asymptotically stable as long as there are symmetric positive definite matrices Q_1 , Q_2 , and nonsingular matrix $\int_0^{T_s} e^{A_s \gamma} d\gamma$, which are able to make Φ negative definite. The proof of Theorem 2 is completed.

Remark 1. Although this paper discusses the unconstrained MPC, the proposed fractional-order compensation algorithm can be directly extended to the constrained MPC. When the system exists both sampling delay and computation delay, we can first estimate the current state $x(k)$ according to (23), and then calculate the control input $u(k+1)$ at the next time $k+1$. Finally, we can keep the calculated $u(k+1)$ and output it at time $k+1$. For the constrained MPC, we can get the optimal solution $u(k+1)$ by solving a quadratic programming problem. As long as the algorithm used to solve the quadratic programming converges within one sampling cycle, the controlled system under the constrained MPC is stable.

5 Simulation results

5.1 Numerical example

Figure 3 presents the topology and parameters of the BUCK converter. u_{in} , u_C , and i_L denote the input voltage, the output voltage, and the current passing through the inductor, respectively. First, in the conduction stage of the switching tube, we can get the state equation as follows:

$$\begin{bmatrix} \dot{i}_L \\ \dot{u}_C \end{bmatrix} = \begin{bmatrix} 0 & -\frac{1}{L} \\ \frac{1}{C} & -\frac{1}{RC} \end{bmatrix} \begin{bmatrix} i_L \\ u_C \end{bmatrix} + \begin{bmatrix} \frac{1}{L} \\ 0 \end{bmatrix} u_{in}. \quad (42)$$

In the shutdown stage of the switching tube, we can obtain

$$\begin{bmatrix} \dot{i}_L \\ \dot{u}_C \end{bmatrix} = \begin{bmatrix} 0 & -\frac{1}{L} \\ \frac{1}{C} & -\frac{1}{RC} \end{bmatrix} \begin{bmatrix} i_L \\ u_C \end{bmatrix} + \begin{bmatrix} 0 \\ 0 \end{bmatrix} u_{in}. \quad (43)$$

Average (42) and (43), and we have

$$\begin{bmatrix} \dot{i}_L \\ \dot{u}_C \end{bmatrix} = \begin{bmatrix} 0 & -\frac{1}{L} \\ \frac{1}{C} & -\frac{1}{RC} \end{bmatrix} \begin{bmatrix} i_L \\ u_C \end{bmatrix} + \begin{bmatrix} \frac{u_d}{L} \\ 0 \end{bmatrix} u_{in},$$

where u_d is the duty cycle. Taking u_d as the control input, we are able to derive the mathematical model of the BUCK converter

$$\begin{bmatrix} \dot{i}_L \\ \dot{u}_C \end{bmatrix} = \begin{bmatrix} 0 & -\frac{1}{L} \\ \frac{1}{C} & -\frac{1}{RC} \end{bmatrix} \begin{bmatrix} i_L \\ u_C \end{bmatrix} + \begin{bmatrix} \frac{u_{in}}{L} \\ 0 \end{bmatrix} u_d.$$

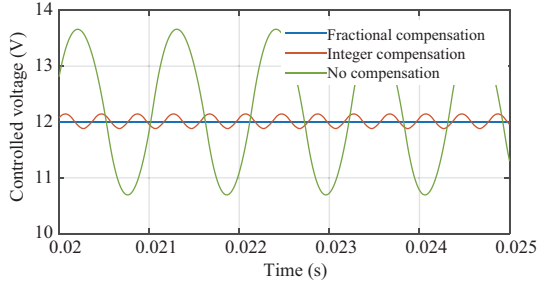


Figure 4 (Color online) Comparison of the sampling delay compensation algorithms under the BUCK converter.

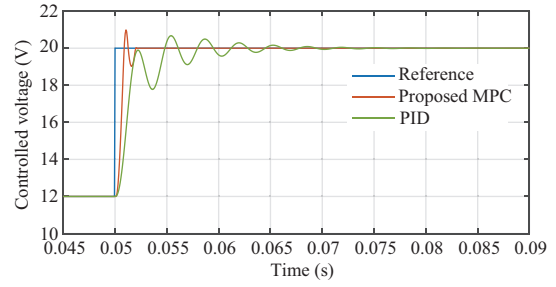


Figure 5 (Color online) Step response of the BUCK converter under the coexistence of computation and sampling delays.

Assuming u_C is the controlled variable and the sampling cycle T_s is $50 \mu\text{s}$, A , B , C , and F in the model (1) are

$$A = \begin{bmatrix} 0.9959 & -0.0162 \\ 0.4870 & 0.9472 \end{bmatrix}, \quad B = \begin{bmatrix} 0.3995 \\ 0.0983 \end{bmatrix},$$

$$C = [0 \ 1], \quad F = \begin{bmatrix} 0 \\ 0 \end{bmatrix}.$$

We compare three MPC methods, namely, no compensation method, integer compensation method [16], and the proposed fractional-order compensation method. Assume that the computation delay d_c is 0 and sampling delay τ is 1.5. The reference value of the controlled variable u_C is 12 V. Figure 4 illustrates that the fractional-order compensation algorithm has a better effect than that of the integer compensation and uncompensated cases.

To further prove the contributions and advantages of the proposed algorithm, we utilize the proportional-integral-differential (PID) algorithm for comparison when the computation delay and sampling delay coexist. The computation delay d_c is 0.9 and sampling signal delay τ is 1.6. Figure 5 presents the step response of the controlled variable using the full compensation algorithm. Moreover, the reference value steps to 20 V from 12 V at 0.05 s. Indeed, the PID algorithm can deal with the problem of fractional-order delay and guarantee that the controlled voltage tracks the reference value. However, the dynamic performance of the PID algorithm is worse than that of the proposed MPC algorithm. The setting time of the PID algorithm is much longer than that of the proposed algorithm. Compared with PID algorithm, MPC performs optimization calculation in each sampling period, which ensures its fast regulating ability [23]. Indeed, the fast regulating speed is significant for fast sampling systems. Accordingly, the great performance of MPC in fast sampling systems makes it capable to deal with the fractional-order delay compensation problem.

5.2 Example of wireless power transfer system

In this subsection, we use the power electronic system in PLECS instead of its mathematical model. In addition, the MPC algorithm runs in MATLAB. Then, we combine MATLAB and PLECS to obtain the simulation results. Therefore, the controlled variable will not be as smooth as the numerical model due to the existence of the switching ripple. According to the wireless charging system model in [24], we change the load of the DC-DC converter into a lithium battery, and remove the output filter capacitor to obtain the structure presented in Figure 6. The DC-DC converter of the wireless power transfer system is modeled as

$$\begin{cases} \dot{x} = A_{s1}x + F_{s1}, & kT_s \leq t < (k + u_d)T_s, \\ \dot{x} = A_{s2}x + F_{s2}, & (k + u_d)T_s \leq t < (k + 1)T_s, \end{cases}$$

where $[kT_s, (k + u_d)T_s)$ and $[(k + u_d)T_s, (k + 1)T_s)$ denote the on and off states of insulated gate bipolar transistor (IGBT), respectively. The switching cycle is consistent with the sampling cycle. $x = [u_{Cd} \ i_{Ld}]^T$

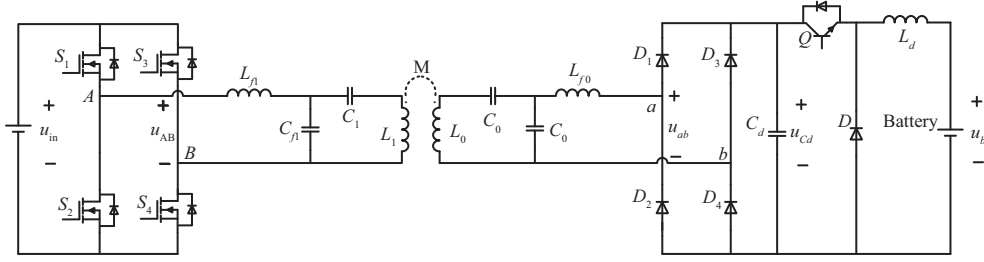

Figure 6 Topology of the wireless power transfer system.

Table 1 Parameters of wireless power transfer

Parameter	Symbol	Value
Input voltage of the inverter	u_{in}	200 V
Self-inductance of the primary-side coil	L_1	178 μ H
Self-inductance of the secondary-side coil	L_0	178 μ H
Primary-side resonant inductor	L_{f1}	45.5 μ H
Secondary-side resonant inductor	L_{f0}	45.5 μ H
Primary-side resonant capacitor	C_{f1}	77.05 nF
Secondary-side resonant capacitor	C_{f0}	77.05 nF
Primary-side compensation capacitor	C_1	24.46 nF
Secondary-side compensation capacitor	C_0	24.46 nF
DC-DC input capacitor	C_d	90 μ F
DC-DC inductor	L_d	3 mH
Battery voltage	u_b	136 V
Sampling cycle	T_s	50 μ s

is the state variable. A_{s1} , A_{s2} , F_{s1} , and F_{s2} are

$$A_{s1} = \begin{bmatrix} 0 & -\frac{1}{C_d} \\ \frac{1}{L_d} & 0 \end{bmatrix}, \quad F_{s1} = \begin{bmatrix} \frac{i_{in}}{C_d} \\ -\frac{u_b}{L_d} \end{bmatrix}, \quad A_{s2} = \begin{bmatrix} 0 & 0 \\ 0 & 0 \end{bmatrix}, \quad F_{s2} = \begin{bmatrix} \frac{i_{in}}{C_d} \\ -\frac{u_b}{L_d} \end{bmatrix}, \quad (44)$$

where i_{in} represents the equivalent DC-DC input current; C_d and L_d are the DC-DC input capacitor and the DC-DC inductor, respectively; u_{Cd} and i_{Ld} are voltage on C_d and current on L_d , respectively; u_b denotes the battery voltage. By discretizing (44), we can obtain

$$\begin{cases} x(k+1) = A_{d1}x(k) + F_{d1}, & u_d = 1, \\ x(k+1) = A_{d2}x(k) + F_{d2}, & u_d = 0. \end{cases}$$

The introduction of the duty cycle u_d brings the nonlinear term to the model as follows:

$$\begin{cases} x(k+1) = A_m x(k) + B_m x(k) u_d + C_m u_d + D_m, \\ A_m = A_{d2}, \quad B_m = A_{d1} - A_{d2}, \\ C_m = F_{d1} - F_{d2}, \quad D_m = F_{d2}. \end{cases}$$

Based on the method outlined by [25], we can obtain the linear model (1).

5.2.1 Influence of the computation delay and sampling delay on the system

Based on parameters in Table 1, we first discuss the influence of the computation delay and sampling delay on the system. If the sampling delay is τ cycle, i.e., the sampled state variable at the current moment is $x(k - \tau)$, then the calculated control law is $u(k - \tau)$, which means that the control law is delayed by τ cycle. If the computation delay is d_c cycle, the control law is delayed by d_c cycle. Indeed, the longer the delay time of the control law is, the greater the influence on the system is.

The computation delay refers to the time spent by the controller in the calculation process, which results in a delay in the control law. In applications, the controller runs through the interrupt service

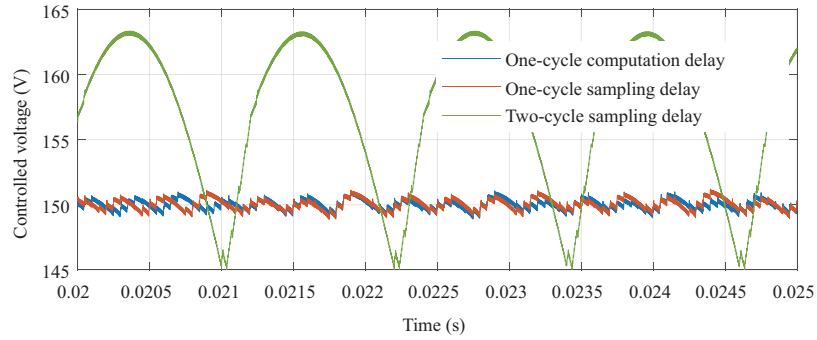


Figure 7 (Color online) Comparison of the influence of the computation delay and sampling delay on the system.

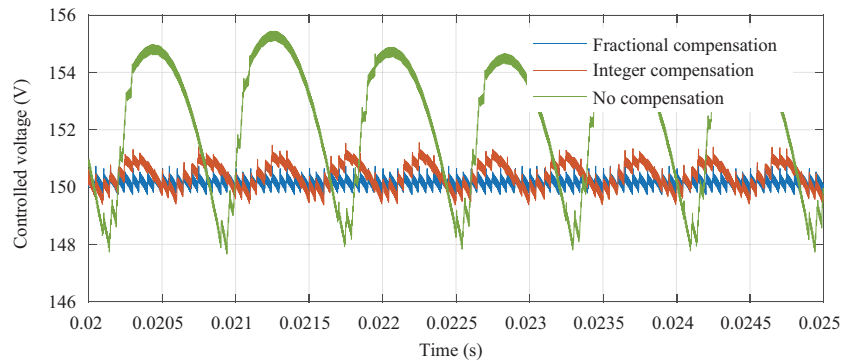


Figure 8 (Color online) Comparison of the sampling delay compensation algorithms under the wireless power transfer system.

function. When the sampling interrupt service function is triggered, the controller starts to execute the control algorithm. When the interrupt service function at the next moment is triggered, the controller will not be able to complete the calculation if its calculation time is greater than one sampling cycle. Therefore, the calculation of the control signal needs to be completed within one cycle. Accordingly, the computation delay will not exceed one sampling cycle. Different from the computation delay, the sampling delay can be greater than one cycle. When the sampling delay is longer than the computation delay, the sampling delay has a greater influence on the system.

We set the reference value and sampling cycle in the wireless power transfer system as 150 V and 50 μs , respectively. Subsequently, we present the influence of one-cycle computation delay, one-cycle sampling delay, and two-cycle sampling delay on the system. As shown in Figure 7, if the computation delay and sampling delay are both one cycle, the controlled voltage variations of the system are basically the same. If the sampling delay is two cycles, the controlled voltage will oscillate more violently than that of the one-cycle computation delay. Accordingly, for the sampling delay and computation delay, the delay with longer time has a greater influence on the system.

5.2.2 Effect of fractional-order compensation algorithm

Figure 8 shows the results of the sampling delay compensation. Assume that the computation delay is 0 μs and the sampling delay is 70 μs , i.e., $d_c = 0$ and $\tau = 1.4$. The system is also tested in three cases: no compensation, integer multiple compensation, and fractional multiple compensation. When the system has no sampling delay compensation, the controlled voltage is oscillatory. When we adopt the integer multiple compensation for the system, the effect of the controlled voltage is improved, but it is still slightly fluctuating. If the fractional compensation is employed in the system, the effect of controlled voltage is great because of its advantage of the precise compensation.

Assume that the computation delay and sampling delay are 40 and 70 μs , respectively, i.e., $d_c = 0.8$ and $\tau = 1.4$. If only one kind of delay is compensated, the control effect is unsatisfactory as shown in Figure 9(a). In addition, the control signal variations are presented in Figure 9(b). The change of control signal is more regular when the algorithm of the full compensation strategy is adopted. The simulation results demonstrate the validity of the proposed fractional-order compensation and the extended hybrid delay compensation strategy. In this hybrid delay state, we further compare the results of the proposed

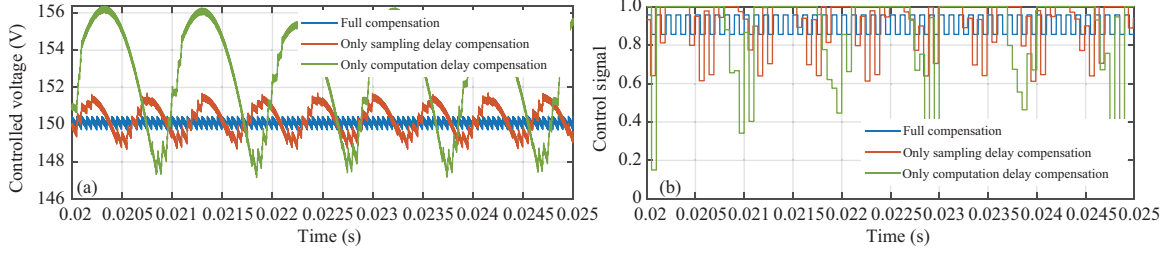


Figure 9 (Color online) Coexistence of computation and sampling delays. (a) Controlled variable variations; (b) control signal variations.

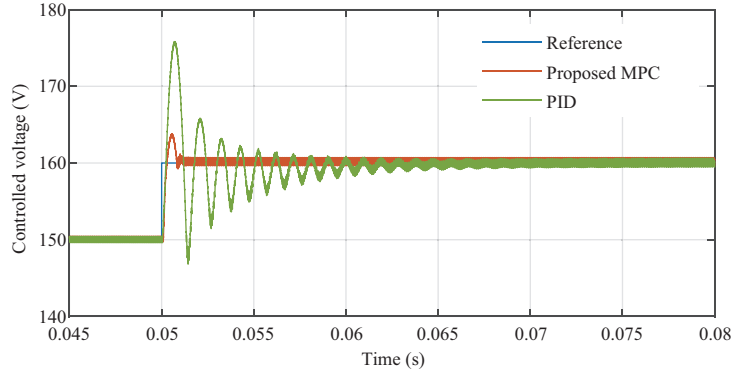


Figure 10 (Color online) Step response of the wireless power transfer system under the coexistence of computation and sampling delays.

MPC and PID algorithms. The reference value steps from 150 to 160 V at 0.05 s. Figure 10 presents that the adjustment speed of the proposed MPC algorithm is faster than that of the PID algorithm. It further proves that the proposed MPC algorithm is superior.

5.2.3 Time-varying situation of F

Now we discuss the situation where F in the system (1) is time-varying. D_F in (11) needs to be revised as follows:

$$D_F = \begin{bmatrix} \sum_{i=-1}^0 CA^{-i}F(k+i+1) \\ \sum_{i=-1}^1 CA^{1-i}F(k+i+1) \\ \vdots \\ \sum_{i=-1}^{N_p-1} CA^{N_p-i-1}F(k+i+1) \end{bmatrix}_{N_p \times 1}.$$

Similarly, the revised $x(k|k-\tau)$ is

$$\begin{aligned} x(k|k-\tau) &= A^N((\alpha_0 I_m + \alpha_1 A^{-1})^{-1}(x(k-\tau) + \alpha_1 A^{-1}(Bu(k-(N+1)) + F(k-(N+1)))) \\ &\quad + \sum_{i=1}^N A^{i-1}Bu(k-i) + \sum_{i=1}^N A^{i-1}F(k-i)). \end{aligned}$$

The general method to deal with time-varying problems is to assume that F in the prediction horizon is constant, and then the MPC rolling optimization mechanism is used to feedback F in real-time. Based on this idea, we assume that the values of time-varying F in the proposed method are the sampled value at the sampling moment. Then, F is updated at each sampling moment through using the MPC rolling optimization mechanism. We consider the voltage expression of the lithium battery as follows:

$$u_b = 136 + 2 \sin(200\pi t).$$

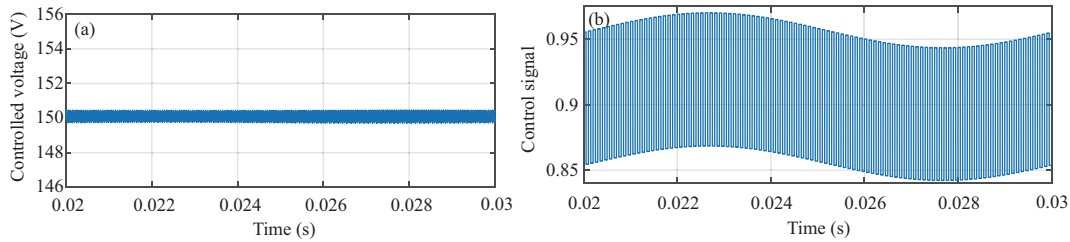


Figure 11 (Color online) Control effect under time-varying situation of F . (a) Controlled variable variations; (b) control signal variations.

Correspondingly, F is time-varying according to (44). The computation delay and sampling delay of the system are set to 40 and 70 μs , respectively; the reference value is 150 V. As presented in Figure 11, the controlled voltage can still be stabilized at 150 V. The approaches in this paper are still applicable. Moreover, the control signal exhibits periodic changes because the lithium battery voltage u_b , the control signal u_d , and the controlled voltage u_{Cd} satisfy the relationship $u_b = u_{Cd} \times u_d$. This relationship is the property of the DC-DC converter. When the lithium battery voltage changes periodically, the control signal also changes periodically to stabilize the controlled voltage.

6 Conclusion

In this paper, we propose an MPC algorithm with a fractional-order delay compensation for delay problems in fast sampling systems. Combined with the idea of an FIR fractional delay filter, we present a sampling delay compensation method with low computational complexity and high accuracy. Considering the coexistence of computational and sampling delays, we design a full delay compensation method. Simulation results show the validity and superiority of the proposed compensation method.

Acknowledgements This work was partially supported by National Key R&D Program of China (Grant No. 2018YFA0703800), Science Fund for Creative Research Group of National Natural Science Foundation of China (Grant No. 61621002), National Natural Science Foundation of China (Grant No. 61873233), Zhejiang Key R&D Program (Grant No. 2021C01198), and Ningbo Science and Technology Innovation 2025 Major Project (Grant No. 2019B10116).

References

- 1 Mayne D Q, Rawlings J B, Rao C V, et al. Constrained model predictive control: stability and optimality. *Automatica*, 2000, 36: 789–814
- 2 Mayne D Q. Model predictive control: recent developments and future promise. *Automatica*, 2014, 50: 2967–2986
- 3 Yoon S Y, Lin Z L. Predictor based control of linear systems with state, input and output delays. *Automatica*, 2015, 53: 385–391
- 4 Teng L, Wang Y Y, Cai W J, et al. Efficient robust fuzzy model predictive control of discrete nonlinear time-delay systems via Razumikhin approach. *IEEE Trans Fuzzy Syst*, 2019, 27: 262–272
- 5 Martins M A F, Yamashita A S, Santoro B F, et al. Robust model predictive control of integrating time delay processes. *J Process Control*, 2013, 23: 917–932
- 6 Bhaskaran A, Rao A S. Predictive control of unstable time delay series cascade processes with measurement noise. *ISA Trans*, 2020, 99: 403–416
- 7 Jeong S C, Park P. Constrained MPC algorithm for uncertain time-varying systems with state-delay. *IEEE Trans Autom Control*, 2005, 50: 257–263
- 8 Liu J F, de la Peña D M, Christofides P D. Distributed model predictive control of nonlinear systems subject to asynchronous and delayed measurements. *Automatica*, 2010, 46: 52–61
- 9 Liu J F, Chen X Z, de la Peña D M, et al. Iterative distributed model predictive control of nonlinear systems: handling asynchronous, delayed measurements. *IEEE Trans Autom Control*, 2012, 57: 528–534
- 10 Teng L, Wang Y Y, Cai W J, et al. Fuzzy model predictive control of discrete-time systems with time-varying delay and disturbances. *IEEE Trans Fuzzy Syst*, 2018, 26: 1192–1206
- 11 Liu Z, Xie L, Bemporad A, et al. Fast linear parameter varying model predictive control of buck DC-DC converters based on FPGA. *IEEE Access*, 2018, 6: 52434–52446
- 12 Falkowski P, Sikorski A. Finite control set model predictive control for grid-connected AC-DC converters with LCL filter. *IEEE Trans Ind Electron*, 2018, 65: 2844–2852
- 13 Guzman R, de Vicuna L G, Camacho A, et al. Receding-horizon model-predictive control for a three-phase VSI with an LCL filter. *IEEE Trans Ind Electron*, 2019, 66: 6671–6680
- 14 Cortes P, Rodriguez J, Silva C, et al. Delay compensation in model predictive current control of a three-phase inverter. *IEEE Trans Ind Electron*, 2012, 59: 1323–1325
- 15 Vafamand N, Khooban M H, Dragicevic T, et al. Networked fuzzy predictive control of power buffers for dynamic stabilization of DC microgrids. *IEEE Trans Ind Electron*, 2019, 66: 1356–1362
- 16 Zhang L Y, Zhou Z, Chen Q H, et al. Model predictive control for electrochemical impedance spectroscopy measurement of fuel cells based on neural network optimization. *IEEE Trans Transp Electrification*, 2019, 5: 524–534
- 17 Lee W R, Caccetta L, Rehbock V. Optimal design of all-pass variable fractional-delay digital filters. *IEEE Trans Circ Syst I*, 2008, 55: 1248–1256

- 18 Kwan H K, Jiang A. FIR, allpass, and IIR variable fractional delay digital filter design. *IEEE Trans Circ Syst I*, 2009, 56: 2064–2074
- 19 Dam H H. Design of variable fractional delay filter with fractional delay constraints. *IEEE Signal Process Lett*, 2014, 21: 1361–1364
- 20 Zou Z X, Zhou K L, Wang Z, et al. Frequency-adaptive fractional-order repetitive control of shunt active power filters. *IEEE Trans Ind Electron*, 2015, 62: 1659–1668
- 21 Bagheri P, Khaki-Sedigh A. Closed form tuning equations for model predictive control of first-order plus fractional dead time models. *Int J Control Autom Syst*, 2015, 13: 73–80
- 22 Laakso T I, Valimaki V, Karjalainen M, et al. Splitting the unit delay [FIR/all pass filters design]. *IEEE Signal Process Mag*, 1996, 13: 30–60
- 23 Zhou Z, Zhang L Y, Liu Z T, et al. Model predictive control for the receiving-side DC-DC converter of dynamic wireless power transfer. *IEEE Trans Power Electron*, 2020, 35: 8985–8997
- 24 Zhou Z, Zhang L Y, Liu Z T, et al. Design and demonstration of a dynamic wireless power transfer system for electric vehicles. *Sci China Inf Sci*, 2019, 62: 224201
- 25 Beccuti A G, Mariethoz S, Cliquennois S, et al. Explicit model predictive control of DC-DC switched-mode power supplies with extended kalman filtering. *IEEE Trans Ind Electron*, 2009, 56: 1864–1874